Maturation of glycinergic inhibition in the gerbil medial superior olive after hearing onset

Anna K. Magnusson[1,2], Christoph Kapfer[2], Benedikt Grothe[1,2] and Ursula Koch[1,2]

[1] *Division of Neurobiology, Department Biologie II, Ludwig-Maximilians-University, Grosshadernerstrasse 2, D-82152 Martinsried, Germany*
[2] *Max Planck Institute of Neurobiology, Am Klopferspitz 18, D-82152 Martinsried, Germany*

The neurones of the medial superior olive (MSO) are the most temporally sensitive neurones in the brain. They respond to the arrival time difference of sound at the two ears with a microsecond resolution; these interaural time differences are used to localize low-frequency sounds. In addition to the excitatory inputs from each ear, the MSO neurones also receive binaural glycinergic projections, which have a critical role in sound localization processing. Recently, it was shown that the glycinergic input to the MSO undergoes an experience-dependent structural reorganization after hearing onset. To explore the maturation of inhibition during the development of sound localization on a cellular level, glycinergic currents and potentials were measured in gerbil MSO principal cells from postnatal (P) day P12–P25 by whole-cell patch-clamp recordings. The synaptic glycinergic currents accelerated to rapid decay kinetics (∼2 ms) and rise times (∼0.4 ms) after hearing onset, reaching maturity around P17. Since the kinetics of miniature glycinergic currents did not change with age, it is likely that a higher degree of transmitter release synchrony is the underlying mechanism influencing the acceleration of the kinetics. During the same period, the synaptic glycinergic potentials accelerated four-fold, largely as a result of a prominent decrease in input resistance. In accordance with a reorganization of the glycinergic inputs, the evoked peak conductances decreased more than two-fold, together with a three-fold reduction in the frequency of miniature events after hearing onset. These age-dependent changes were absent in animals that had been reared in omni-directional noise, indicating that an experience-dependent pruning of synaptic inputs is important for the maturation of functional inhibition in the MSO. Taken together, these striking developmental adjustments of the glycinergic inhibition in the MSO most probably reflect an adaptation to improve the encoding of auditory cues with great temporal precision and fidelity during the maturation of sound localization behaviour.

(Resubmitted 15 July 2005; accepted 5 August; first published online 11 August 2005)
Corresponding author A. K. Magnusson: Division of Neurobiology, Department Biologie II, Ludwig-Maximilians-University, Grosshadernerstrasse 2, D-82152 Martinsried, Germany. Email: magnusson@zi.biologie.uni-muenchen.de

Interaural time differences (ITDs) of sounds arriving at the two ears are the main cues mammals use to localize low-frequency sounds. The underlying neural circuitry has the highest temporal resolution in the mammalian brain and can resolve ITDs of as low as 30 μs on a single-cell level (Skottun, 1998). The medial superior olive (MSO) is the initial site of ITD detection in the mammalian brain (Goldberg & Brown, 1969; Yin & Chan, 1990; Spitzer & Semple, 1995; Brand *et al.* 2002). It has traditionally been thought that ITDs are encoded by coincidence detection of solely excitatory inputs, which terminate on the respective dendrites of the bipolar MSO principal cells (Cant & Benson, 2003). However, numerous studies provide ample evidence for a strong glycinergic inhibitory input (Adams & Mugnaini, 1990; Grothe & Sanes, 1993; Grothe & Sanes, 1994; Smith, 1995, 2000; Brand *et al.* 2002). An anatomical substrate for this inhibition exists as the MSO receives bilateral inhibitory projections from the medial and the lateral nuclei of the trapezoid body (MNTB and LNTB) (Cant & Hyson, 1992; Kuwabara & Zook, 1992). These structures exhibit several striking morphological and physiological specializations, critical to fast and temporally precise neural transmission, such as the MNTB input synapse – the calyx of Held, which is the largest and fastest synapse in the brain (von Gersdorff & Borst, 2002). Recently, *in vivo* recordings from the gerbil MSO demonstrated that the glycinergic inhibition is of major importance for tuning the ITD sensitivity to the animals' physiological needs, determined by their head size (Brand *et al.* 2002). Taken together, these findings suggest that

© The Physiological Society 2005 DOI: 10.1113/jphysiol.2005.094763

the MSO neurones are influenced by a very fast and phase-locked glycinergic inhibition that adjusts their sensitivity to ITDs (Grothe, 2003; McAlpine & Grothe, 2003). The logical question that then arises is how fast the glycinergic inhibition is in the MSO and if it is uniquely specialized to meet the temporally precise requirements of ITD processing. There is currently no evidence for a glycinergic inhibition with kinetics in the submillisecond range in other parts of the central nervous system. Moreover, a study of the glycinergic synaptic currents prior to and around hearing onset at postnatal (P) day 12 in the MSO of the rat, a predominantly high-frequency hearing animal, indicate that the currents do not meet the required speed necessary to substantiate such a fast inhibition (Smith *et al.* 2000).

Interestingly, the inhibitory inputs undergo a structural reorganization after hearing onset when MSO glycine receptors are refined to an almost purely somatic location in the gerbil, a mammal with excellent low-frequency hearing (Kapfer *et al.* 2002). It has been speculated that the somatic arrangement of glycinergic inputs improves the temporal accuracy of the MSO neurones and provides the basis for a fast functional inhibition, as implied by the *in vivo* experiments (Clark, 1969; Kapfer *et al.* 2002). This late developmental reorganization is unusual, as many processes related to the maturation of the mammalian auditory system have been shown to take place before hearing onset, when inhibitory inputs are depolarizing (Kandler, 2004). Moreover, these structural changes are dependent on a normal acoustic experience during and shortly after hearing onset, as they are impaired by rearing the animals in omnidirectional noise or by cochlear ablations during this critical period (Kapfer *et al.* 2002).

In the present study we analysed the developmental changes of the glycinergic MNTB–MSO synapse in the gerbil after hearing onset (P12–P25), a time period when auditory experience provides the binaural features necessary for the full maturation of ITD processing. These results were also used to clarify the kinetics of the inhibitory input contributing to the ITD-detection circuitry. Further, to investigate the mechanisms underlying the experience-dependent reorganization of this glycinergic circuit, we measured the effects of omnidirectional noise exposure during hearing onset on the development of the inhibition.

Methods

Slice preparation

Transverse brainstem slices in the area of the superior olivary complex were prepared from gerbils (*Meriones unguiculatus*) aged P12–P25 (Fig. 1*A*). The animals were decapitated under isofluorane anaesthesia in conformity with the rules set by the EC Council Directive (86/89/ECC) and German animal welfare legislation. Subsequently, the brainstem was carefully removed and placed in ice-cold low sodium, high sucrose artificial cerebrospinal fluid (aCSF, see below). Slices with a thickness of 170–300 μm were cut in the rostral direction from the level of the facial nerve, with a vibratome (VT1000S; Leica, Wetzlar, Germany), and incubated at 32°C in normal aCSF (see below) for 20–60 min, after which they were allowed to cool to room temperature. Recordings were obtained within 4–5 h of the preparation. Lucifer Yellow (0.1%) was added to the pipette solution to aid online identification of the cell morphology and the recording site with a fluorescence-sensitive camera (AxioCam, MRm, Zeiss, Oberkochen, Germany). In some cases neurobiotin (0.1%) was added to the pipette solution and the morphology was confirmed by means of standard immunohistochemistry using a Cy3-Streptavidin antibody solution (1 : 800; Dianova, Germany) and, subsequently, a laser-scanning confocal microscope (TCS 4D, Leica, Wetzlar, Germany). Only MSO principal cells, with a bipolar shape and with their somata arranged in one parasagittal plane (Fig. 1*B*), were included in this study.

Solutions and drugs

The low-sodium, high-sucrose aCSF contained (mM): 85 NaCl, 2.5 KCl, 1.25 NaH_2PO_4, 25 $NaHCO_3$, 75 sucrose, 25 glucose, 0.5 $CaCl_2$, 4 $MgCl_2$ and 0.5 ascorbic acid whereas the normal aCSF contained (mM): 125 NaCl, 2.5 KCl, 1.25 NaH_2PO_4, 26 $NaHCO_3$, 25 glucose, 2 $CaCl_2$ and 1 $MgCl_2$. The external solutions were bubbled continuously with carbogen gas (95% O_2–5% CO_2), generating a pH of 7.4.

For current-clamp recordings the internal pipette solution contained (mM): 130 K-gluconate, 5 KCl, 10 Hepes, 1 EGTA, 2 Na_2-ATP, 2 Mg-ATP, 0.3 Na_3-GTP, 10 Na_2-phosphocreatinine, adjusted to pH 7.3 with KOH. For voltage-clamp recordings Cs-based internal solutions with low, medium and high chloride concentrations were used. The various chloride concentrations were achieved using $CsMeSO_4$, CsCl or a mixture of both, giving rise to a final $[Cl^-]_i$ of 7, 54 and 144 mM. The low-chloride solution contained (in mM): 130 $CsMeSO_4$, 10 Hepes, 1 EGTA, 5 NaCl, 1 $CaCl_2$, 2 Mg-ATP, 0.3 Na_3-GTP, 10 Na_2-phosphocreatinine, adjusted to pH 7.3 with CsOH. The medium and high chloride solutions contained (mM): 75 (medium chloride solution) $CsMeSO_4$, 50 or 140 CsCl, 10 Hepes, 10 EGTA, 2 NaCl, 1 $CaCl_2$, 2 Mg-ATP, 0.3 Na_3-GTP, adjusted to pH 7.3 with CsOH. The external $[Cl^-]$ was continuously 133.5 mM. QX-314 (5 mM) was added to the medium- and high-chloride solutions before usage in order to obviate postsynaptic voltage-gated sodium currents. For perforated-patch recordings, the pipette solution contained (mM): 135 KCl, 10 Hepes, 1 EGTA, adjusted to pH 7.3.

The following pharmacological agents were used: 6-cyano-7-nitroquinoxaline-2,3-dione (CNQX),

© The Physiological Society 2005

6,7-dinitroquinoxaline-2,3-dione (DNQX), (±)2-amino-5-phosphono-pentanoic acid (D-APV), (+)MK-801 maleate, 5,7-dichlorokynurenate, SR95531, ZD7288, SCH50911 and tetrodotoxin (TTX) (all Tocris-Cookson, Bristol, UK), QX-314, Lucifer Yellow, gramicidin, strychnine (all Sigma-Aldrich, Deisenhofen, Germany) and neurobiotin (Vector, Burlingham, CA, USA). All drugs were dissolved in dH_2O (10 mM), stored at −20°C, and diluted and added to the perfusate during the experiment.

Recording procedures

Slices were transferred to a recording chamber perfused (3–5 ml min^{-1}) with oxygenated aCSF at 32 ± 2°C. The putative MSO principal cells were viewed with an upright microscope (Zeiss Axioscope, Oberkochen, Germany) using a 40× water-immersion objective (Achroplan, Zeiss) and infrared-differential interference optics equipped with an infrared-sensitive digital camera (KP-M2R, Hitachi Kokusai Electric, Tokyo, Japan).

Whole-cell current- and voltage-clamp recordings were performed from the MSO with a Multiclamp 700A amplifier (Axon Instruments, Union City, CA, USA). Borosilicate glass microelectrodes (GC150F-10, Harvard Apparatus, Edenbridge, UK) were pulled on a vertical electrode puller (PP-830, Narashige, Tokyo, Japan), yielding a final tip resistance of 4–10 MΩ for current- or 2.5–5 MΩ for voltage-clamp recordings.

The bridge balance was applied for current-clamp recordings. For voltage-clamp recordings, the series resistance (mean 10.8 ± 2.7 MΩ, $n = 97$ and maximum = 15.3 MΩ) was compensated by 70–90% (lag of 10–16 μs) and monitored throughout the experiment. The series resistance was not allowed to vary by more than 10%. In the vast majority of voltage-clamp recordings the low [Cl^-] Cs-based internal patch-solution was used with a holding potential of −49 to −59 mV. In some experiments, the medium [Cl^-] or high-[Cl^-] Cs-based internal solution was used during which a holding potential of −70 mV was applied. As there was no difference in the kinetics between the currents recorded with the low and medium [Cl^-], the data were pooled. All voltages have been corrected for the junction potentials (mV): 11.6 K-gluconate; 9 $CsMeSO_4$; 0.6 $CsMeSO_4$/CsCl and 0.9 CsCl.

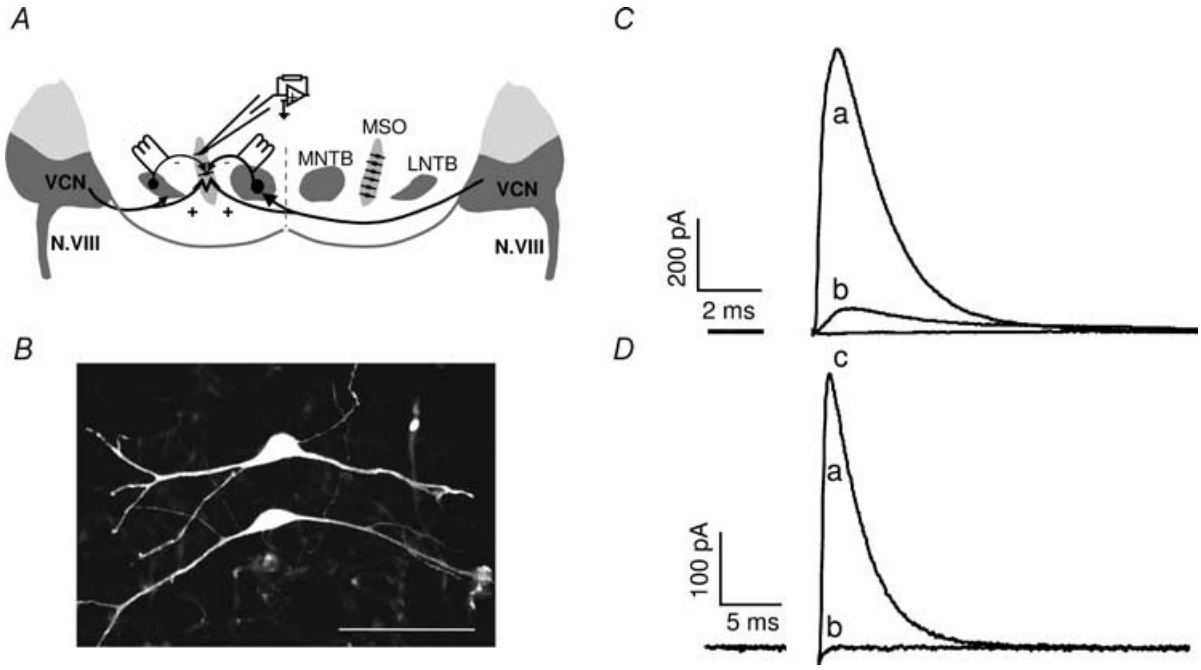

Figure 1. Schematic diagram of the inhibitory connections of MSO principal cells and the glycinergic origin of the inhibition

A, transverse brainstem slices containing the MSO and its two major inhibitory connections from the MNTB and the LNTB were used for patch-clamp recordings from the principal cells. The inhibitory MNTB or LNTB fibres were stimulated using an agar-bridge glass microelectrode filled with 2 M NaCl. *B*, a confocal image of two neurobiotin-filled MSO principal cells from a P17 gerbil. The cells were bipolar and characteristically arranged in one parasagittal plane. *C*, averaged traces of evoked IPSCs before (*a*) and after (*b*) blockade by the glycine receptor antagonist strychnine (0.5 μM) in a P12 gerbil. The residual component was blocked (c) with the $GABA_A$ receptor antagonist SR95531 (5 μM). *D*, averaged traces of evoked IPSCs before (*a*) and after (*b*) complete blockade by strychnine (0.5 μM) in a P14 gerbil. The sample records which represent an average of >20 responses have been superimposed with respect to the baseline current and the timing of the stimulus artefact. The stimulus artefact has been deleted. Scale bar, 100 μm.

© The Physiological Society 2005

Experimental procedures

Evoked synaptic responses were elicited with an agar-bridge glass microelectrode filled with 2 M NaCl, or in some cases with a tungsten bipolar stimulation electrode (Fredrick Haer Corporation, Bowdoinham, ME, USA), which was positioned in the ipsilateral MNTB fibre tract (or in a few cases the LNTB fibre tract) (Fig. 1*A*). A bipolar (+/−) stimulus was triggered by an analog isolated pulse generator (BSI 950, Dagan Corporation, Minneapolis, MN, USA) at a rate of 0.1–0.3 Hz. The threshold stimulus strength was typically 20–100 V or 2–10 mA, with a duration of 20–100 μs stimulus^{-1}. Scaling of the evoked response amplitude for different stimulus intensities was observed in the majority of the neurones over the entire age range.

To enable better visibility, thinner slices (170–200 μm) were used in animals older than P16, whereas thicker slices were used in younger animals (250–300 μm). For the maximal stimulation protocol a slice thickness of 200–250 μm was used for all ages investigated. Results showed that the maximal peak conductance was not altered significantly by the slice thickness, and so the data were pooled.

The evoked glycinergic inhibitory postsynaptic potentials (IPSPs) and currents (IPSCs) were isolated by addition of 10 μM CNQX or 10 μM DNQX, 50 μM D-APV, 5 μM MK-801, 5 μM SR95531 and 10 μM ZD7288 (the latter during voltage-clamp recordings) to the aCSF. Without the $GABA_A$ receptor antagonist SR95531, the synaptic response at P14–P25 was exclusively glycinergic, as it was completely blocked by strychnine (0.5 μM) ($n = 12$) (Fig. 1*D*). However, at P12, a minor GABAergic component was present, which could be blocked by SR95531 ($n = 3$) (Fig. 1*C*). The IPSCs were recorded along the entire rostrocaudal to dorsoventral axis of the MSO. As there was no apparent difference in the inhibitory responses from various subregions the data were pooled.

Isolation of evoked excitatory postsynaptic synaptic currents (EPSCs) was achieved by addition of 5 μM SR95531 and 0.5 μM strychnine to the aCSF. Miniature glycinergic IPSCs (mIPSCs) were recorded with a high [Cl^-] Cs-based internal patch-solution in the presence of 1 μM TTX. The wash-in of the drugs was monitored carefully before data were collected. In recordings obtained with CsCl-based solutions, during which the EPSCs and IPSCs have the same polarity, the drugs were washed through for several minutes before data were collected. For perforated-patch recordings, a stock of gramicidin in DMSO (5 mg ml^{-1}) was freshly prepared before each experiment and prior to the recordings, diluted in the pipette solution to a final concentration of 100 μg ml^{-1}. The tips of the patch-pipettes were filled with a gramicidin-free solution. Recordings were obtained when the series resistance was below 30 MΩ and a compensation of 90% could be achieved. To improve voltage control in the negative range ZD7288 was applied to block the hyperpolarization activated current I_h.

In conductance-clamp experiments, simulated inhibitory conductances (IPSGs) were injected into MSO principal cells from P12 and P17 with an SM-1 amplifier (Cambridge Conductance, Cambridge, UK). The Cl^- reversal potential, estimated for the K-gluconate patch-solution used (see above), was set to −86 mV. The kinetics of the injected IPSGs were based on recorded IPSCs (P12: decay time constant (τ_{decay}) = 5 ms and 10–90% rise time = 1 ms; P20: τ_{decay} = 2 ms and 10–90% rise time = 0.5 ms). The amplitude of the injected conductance was adjusted during the experiment to match the evoked response.

Voltage-clamp control

In order to estimate the quality of the voltage clamp during the IPSC recordings, the time-course of excitatory postsynaptic synaptic currents (EPSCs), which can be extremely fast in mature neurones (Raman *et al.* 1994; Wall *et al.* 2002), was analysed in a number of cells at P17. Since excitatory synapses in MSO principal cells are electrotonically further away from the soma than the inhibitory synapses (Kapfer *et al.* 2002), they would be more subjected to attenuation and distortion of their temporal characteristics during an insufficient voltage clamp than the inhibitory ones. Pharmacologically isolated evoked EPSCs displayed very fast kinetics with a τ_{decay} of 0.48 ± 0.07 ms and a 10–90% rise time of 0.25 ± 0.03 ms (mean ± S.D. $n = 5$). The spontaneous EPSCs, recorded in the same cells, were even faster with a τ_{decay} of 0.30 ± 0.07 ms (mean ± S.D., $P = 0.05$) and a 10–90% rise time of 0.20 ± 0.03 ms (mean ± S.D., $P = 0.08$). Hence, it is unlikely that the IPSC kinetics recorded in this study were significantly slowed down by an insufficient voltage clamp of the cells.

Noise exposure

The gerbils ($n = 11$) were exposed to noise between P7 (five days before hearing onset) and P20 in a cage that was placed in a 100 × 80 × 80 cm sound-attenuated box in a quiet room. White noise from two analog generators (Rhode & Schwarz) was introduced via 12 sets of speakers (two high- and two low-frequency speakers on each of the six sides). Noise from two different sources was thus presented from each direction. The amplitude of the noise was about 80 dB SPL (rms-value, averaging time 30 s) and never exceeded 85 dB SPL. This noise level masks most spatial acoustic cues (Withington-Wray *et al.* 1990), but does not cause any damage to the cochlea or the primary auditory centres (Withington-Wray *et al.* 1990).

© The Physiological Society 2005

The animals' general condition was supervised with an inbuilt video camera system and no signs of stress or abnormal behaviour could be detected during the time of noise exposure. Food and water were provided *ad libitum*.

Data acquisition and analysis

The signals were filtered with a low-pass 4-pole Bessel filter at 10 kHz, sampled at 20–100 kHz and digitized using a Digidata 1322A interface (Axon Instruments). Stimulus generation, data acquisition and offline analysis of data were performed using the pClamp Software (Version 9.0, Axon Instruments). Figures which display averaged evoked responses consist of at least 20 traces. The decays of the evoked and spontaneous IPSCs and EPSCs were fitted using a standard single exponential function (the Chebyshev method) as judged from the correlation coefficient, which was >0.95 for all functions. The mIPSCs were detected with a template search function and each event was subsequently fitted with a single exponential function from which the average decay time constant was derived. The membrane time constant ($\tau_{membrane}$) was estimated by fitting a single exponential function to the voltage change in response to a 100 pA square pulse current. The input resistance (R_{in}) was estimated from the slope of current–voltage plots within a range of -100 to 100 pA and the membrane capacitance ($C_{membrane}$) from the formula: $\tau = R \times C$.

Results are expressed as mean $\pm$ standard deviation (S.D.) in the text and as mean $\pm$ 95% confidence intervals (CI) in the figures and the table. The level of significance was determined by regression analysis and the Pearson test or by Student's unpaired t test ($P < 0.05$ was considered statistically significant). Unless stated otherwise, P-values in the text are obtained by using Student's unpaired t test.

Results

The evoked glycinergic synaptic currents accelerate after hearing onset

The IPSCs in MSO principal cells, evoked by stimulating the MNTB fibres at ~2 times threshold, accelerated significantly during the first week after hearing onset (Fig. 2). Figure 2*A* shows representative IPSCs at an age

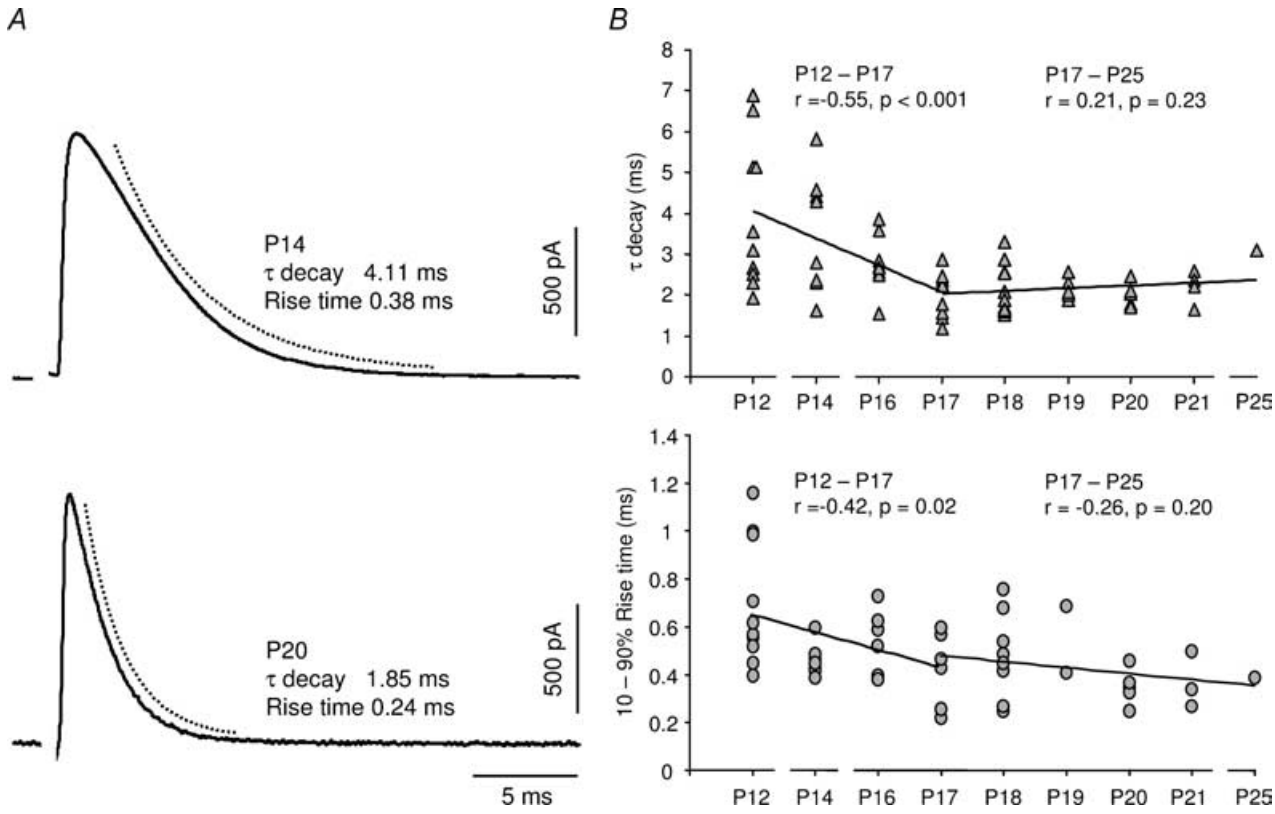

Figure 2. Development of the IPSC kinetics after hearing onset
A, examples of IPSCs from gerbils aged P14 and P20. The decay time-course was estimated by fitting a single exponential function to the response (broken line). Sample records represent an average of 20 responses. The stimulus artefact has been deleted. *B*, developmental changes of the IPSC τ_{decay} and the 10–90% rise time after hearing onset. The continuous lines represent linear regression fits of P12–P17 and P17–P25 data, respectively. The *P*-values were obtained with the Pearson test. Each value in the diagrams was based on an average of $\geq$20 evoked responses.

© The Physiological Society 2005

relatively soon after hearing onset (P14) and at a more mature age (P20). On average, the decay time constant (τ_{decay}) of the IPSCs decreased from 4.0 ± 1.8 ms (P12, mean ± s.d., $n = 10$) to 2.0 ± 0.5 ms (P17, mean ± s.d., $n = 10$, $P = 0.004$) when measured at 32°C (Fig. 2*B*). There was no further significant difference in the τ_{decay} after P17 up to an age of P25 (Fig. 2*B*). Correspondingly, the 10–90% rise time of the glycinergic IPSCs decreased from 0.7 ± 0.3 ms (P12, mean ± s.d., $n = 10$) to 0.45 ± 0.16 ms (P17, mean ± S.D, $n = 7$, $P = 0.04$) after hearing onset. Some IPSCs (27%), from P17 and onwards, displayed extremely fast 10–90% rise times of less than 0.3 ms (Fig. 2*A* and *B*). For all ages there was no correlation between the τ_{decay} and the amplitude of the evoked responses ($r = 0.07$; $P = 0.55$, Pearson test), indicating that the decay of the currents is dependent on neither the amount of transmitter released nor the number of glycine receptors that are activated. In order to be able to relate the kinetics of the glycinergic currents to the *in vivo* condition, the IPSCs of P17 MSO neurones were also measured at 36°C, which is the physiological brain temperature in gerbils (Kimura *et al.* 2002). Neither the τ_{decay} (2.0 ± 0.48 ms; mean ± s.d., $n = 5$, $P = 0.99$) nor the 10–90% rise times (0.53 ± 0.23 ms; mean ± s.d., $n = 5$, $P = 0.52$) of the IPSCs at 36°C were significantly different from the ones recorded at 32°C.

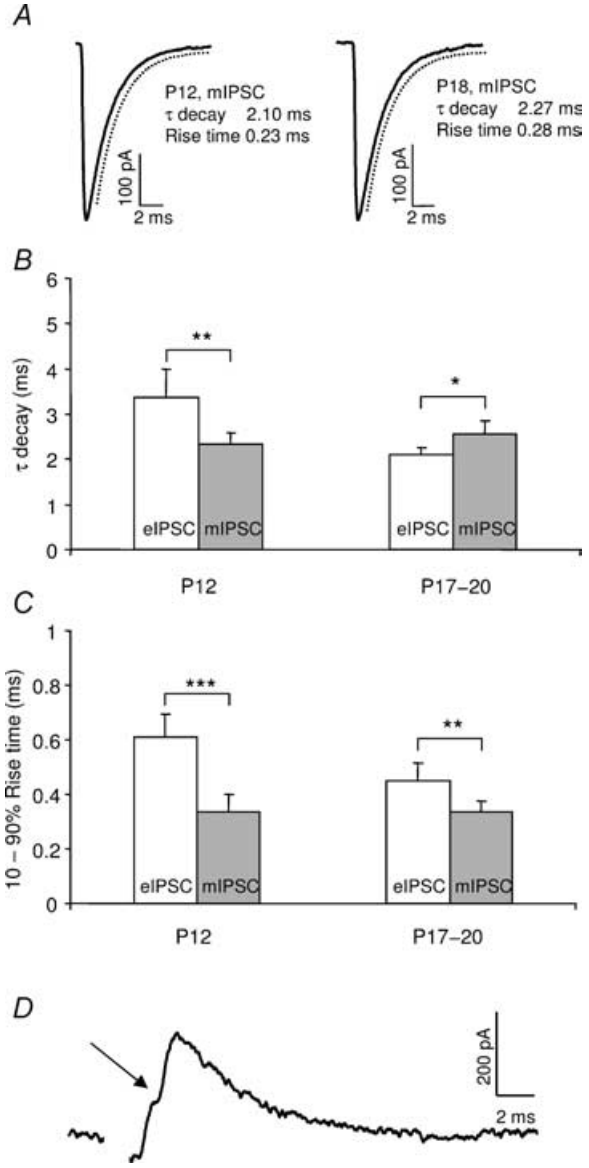

Figure 3. The time-course of miniature IPSCs (mIPSCs) and evoked IPSCs (eIPSCs)
A, the time-course of the averaged response of mIPSCs recorded with a high-[Cl^-] internal solution and in the presence of TTX (1 μM) in a P12 and a P18 gerbil. The decay time-course was estimated by fitting a single exponential function to the response (broken line). *B*, the mean τ_{decay} of mIPSCs at P12 ($n = 11$) and at P17–P20 ($n = 20$) and eIPSCs at P12 ($n = 5$) and at P17–P20 ($n = 30$). *C*, the corresponding mean 10–90% rise time of eIPSCs and mIPSCs at the same ages. A minimal stimulation protocol was used in the P12 animals. *D*, example of a single evoked IPSC response at P12. Note the inflection (arrow) on the rise of the event. Error bars represent 95% confidence intervals. The stimulus artefact has been deleted. $^*P < 0.05$, $^{**}P < 0.01$, $^{***}P < 0.001$.

Transmitter release synchrony increases after hearing onset

Developmental speeding of synaptic currents has been correlated with an increase in the release synchrony of transmitter quanta (Chuhma & Ohmori, 1998; Taschenberger & von Gersdorff, 2000; Wall *et al.* 2002). To investigate whether this can account for the observed acceleration of the inhibitory currents in the MSO, spontaneous miniature IPSCs (mIPSCs) were isolated and recorded in the presence of TTX in P12 and P17–P20 animals and compared to evoked IPSCs (Fig. 3). There was no difference between the kinetics of the mIPSCs in the young and the more mature animals (τ_{decay}: $P = 0.37$; 10–90% rise time: $P = 0.95$). The mIPSCs showed a single exponential decay in both age groups (Fig. 3*A*) and had a τ_{decay} of 2.3 ± 0.5 ms at P12 (mean ± s.d., $n = 11$) and 2.5 ± 0.70 ms at P17–P20 (mean ± s.d., $n = 20$). The corresponding values for the 10–90% rise time were 0.34 ± 0.11 ms at P12 and 0.33 ± 0.09 ms at P17–P20. Hence, the glycine receptor properties seem to remain constant during the period studied. Conversely, at P12, the evoked IPSCs, triggered by minimal stimulation (more than 60% response failure rate), were significantly slower than the mIPSCs (τ_{decay}: $P = 0.0016$; 10–90% rise time: $P < 0.001$), indicating asynchronous release of glycine (Fig. 3*B* and *C*). This is supported by the fact that subsets of events recorded at P12 had inflections of the same size as the mIPSCs on the rise of the evoked response, which probably represent asynchronous release of transmitter quanta (Fig. 3*D*). At more mature ages, kinetics of eIPSCs and mIPSCs were much more similar, even though the rise times were still slower in the evoked IPSCs than in the mIPSCs at P17–P20 ($P = 0.006$)

© The Physiological Society 2005

(Fig. 3*C*). Taken together, these data suggest an increase in the synchrony of transmitter release after hearing onset.

The developmental acceleration of glycinergic potentials is correlated to a steep decrease in input resistance

In order to investigate whether the developmental speeding of the glycinergic currents is paralleled by an acceleration of the inhibitory potentials, IPSPs were recorded in P12–P20 gerbils. The IPSP kinetics accelerated significantly during the first week after hearing onset (Fig. 4). There was a four-fold decrease in the half-width of the IPSPs from 11.8 ± 5.2 ms (P12, mean ± s.d., $n = 7$) to 3.1 ± 1.2 ms (P20, mean ± s.d., $n = 6$, $P = 0.002$) (Fig. 4*B*). This pattern reached maturity around P17, after which no further decrease was observed (Fig. 4*A* and *B*). Further, the 10–90% rise time decreased from 2.1 ± 0.71 (mean ± s.d., $n = 7$) to 1.0 ± 0.60 (mean ± s.d., $P = 0.02$) for the same ages, and stabilized around P17 (Fig. 4*A* and *C*).

Since IPSP kinetics are strongly dependent on the membrane time constant ($\tau_{membrane}$) of a neurone, the developmental changes of $\tau_{membrane}$ were analysed using current step injections around the resting potential. There was a pronounced decrease in the $\tau_{membrane}$ during the first few days after hearing onset (Fig. 5*A*). A further decrease in the $\tau_{membrane}$ was detected up to an age of P17, when the neurones reached maturity (Fig. 5*A*). On average, the $\tau_{membrane}$ decreased from 2.51 ± 1.24 ms (P12, mean ± s.d., $n = 13$) to 0.76 ± 0.56 ms (P17, mean ± s.d., $n = 18$, $P < 0.001$). As expected, the correlations between decreases of the $\tau_{membrane}$ and the half-width ($r = 0.89$; $P < 0.001$, Pearson test), as well as between the $\tau_{membrane}$ and the 10–90% rise time ($r = 0.65$; $P < 0.001$, Pearson test), were highly significant.

The $\tau_{membrane}$ is dependent on the input resistance (R_{in}) and the membrane capacitance ($C_{membrane}$) of a neurone. The values for R_{in}, derived from the same experiments, showed a near identical development to the $\tau_{membrane}$ (Fig. 5*B*). On average, the R_{in} decreased from 53 ± 27 MΩ (P12, mean ± s.d., $n = 13$) to 10 ± 9 MΩ (P17, mean ± s.d., $n = 18$, $P < 0.001$). In contrast, there was no significant change of the estimated $C_{membrane}$ between P12 (83 ± 79 pF; mean ± s.d., $n = 14$) and P17–P20 (89 ± 71 pF; mean ± s.d., $n = 30$, $P = 0.80$). This suggests that the pronounced reduction of the $\tau_{membrane}$ is highly related to the R_{in} of these neurones rather than capacitance changes. Interestingly, in more mature gerbils (P17–P20), several principal cells had an extremely low R_{in} (<1 MΩ). An example is shown in Fig. 5*C*, in which step current injections from –2 nA to 2 nA resulted in extremely small voltage deflections, indicating a presence of strong inward and outward rectifying conductances. Hence, the developmental speeding of the synaptic currents is paralleled by a strong decrease of R_{in} after hearing onset, providing a fast functional inhibition to MSO neurones.

Reorganization of glycinergic inputs does not accelerate IPSP kinetics

The structural reorganization of the glycinergic inputs, from the dendrites to the soma of the MSO principal

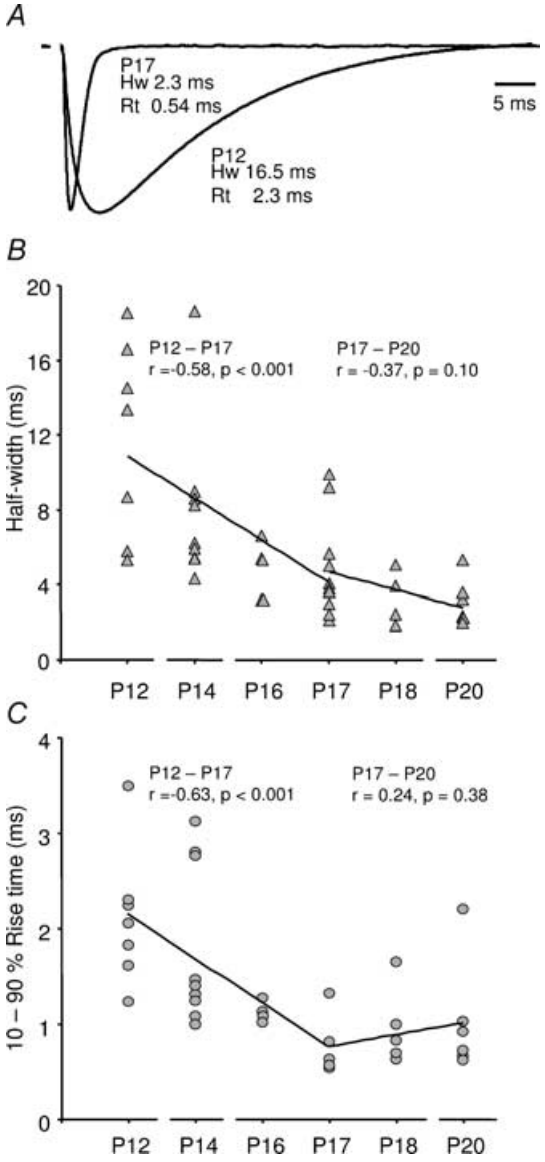

Figure 4. Developmental changes of the IPSP kinetics after hearing onset
A, examples of evoked IPSPs, with half-widths (Hw) and 10–90% rise times (Rt), from P12 and P17 gerbils. The sample records represent an average of 21 responses and have been normalized to their peak amplitudes. The stimulus artefact has been deleted. The developmental time-course of *B*, the IPSP half-width and *C*, 10–90% rise time after hearing onset. The continuous lines represent linear regression fits of P12–P17 and P17–P20 data, respectively. The *P*-values were obtained with the Pearson test. Each value in the diagrams was based on an average of ≥20 evoked responses.

© The Physiological Society 2005

cells, which occurs after hearing onset, might obviate active and passive dendritic filtering and thus contribute to the shortening of IPSPs after hearing onset (Kapfer *et al.* 2002). To investigate this, inhibitory conductances, with the kinetics derived from the averaged IPSCs recorded at P12 and P20, were injected into the soma of MSO neurones. The time-course of IPSPs induced by somatic conductance injection were compared to IPSPs evoked by MNTB fibre stimulation at hearing onset (P12), when the glycine receptors are still present on both the soma and the dendrites, and at a more mature age (P20), when the inhibitory inputs have been reorganized. The half-widths of the two types of IPSP were very similar at P12 ($n = 4$, p = 0.37) (Fig. 6*A* and *B*). This was also the case for the IPSPs recorded at P20 ($n = 4$, $P = 0.92$), which was expected as the inhibition should act directly on the soma in both cases (Fig. 6*B*). As differences in the IPSP time-course, induced by passive and active conductances on the dendrite, were not resolvable in these experiments, the removal of dendritic glycine receptors seems to have a negligible contribution to the developmental acceleration of the IPSPs.

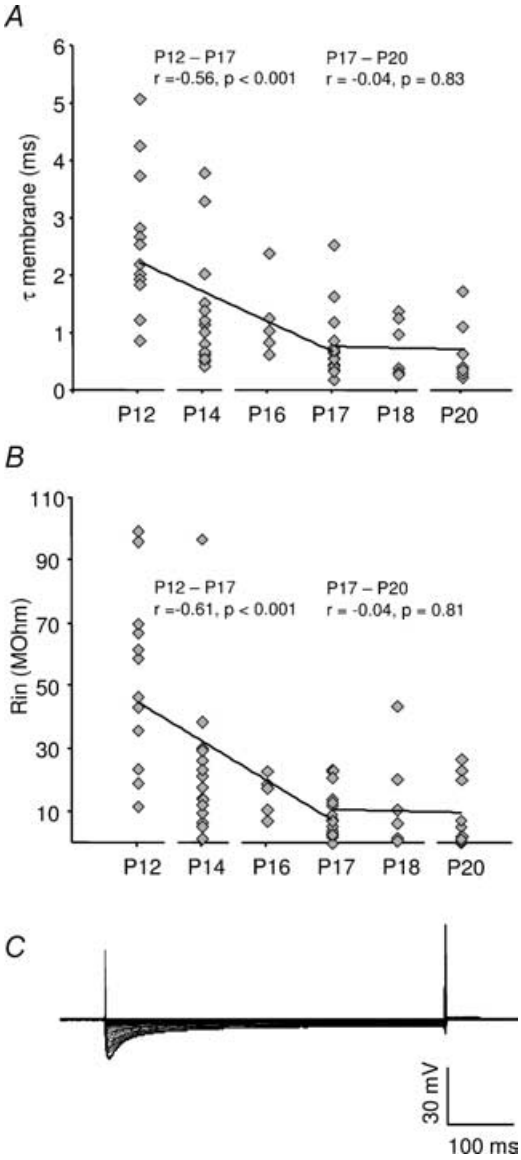

Figure 5. The development of membrane properties in the MSO principal cells
A, the membrane time constant ($\tau_{membrane}$) and *B*, the input resistance (R_{in}) *versus* age after hearing onset in gerbils. The continuous lines represent a linear regression fits of P12–P17 and P17–P25 data, respectively. The *P*-values were obtained with the Pearson test. *D*, the response to hyperpolarizing and depolarizing current step injections (100 pA intervals) from −2 nA to 2 nA in a P17 MSO principal cell. The resting membrane potential was −59 mV.

The resting membrane potential and the glycine reversal potential are mature at hearing onset

Many developmental changes in the lateral superior olive (LSO) seem to be completed before hearing onset (Kandler, 2004). To investigate whether this was also the case in the MSO, the maturation of basic membrane properties, such as the resting membrane potential (V_{rest}) and the glycinergic reversal potential ($E_{glycine}$) were measured from P12–P21. The V_{rest} is mature in the MSO principal cells at hearing onset as there was no ontogenetic difference throughout the period studied ($r = 0.09$; $P = 0.47$, Pearson test). The average V_{rest}

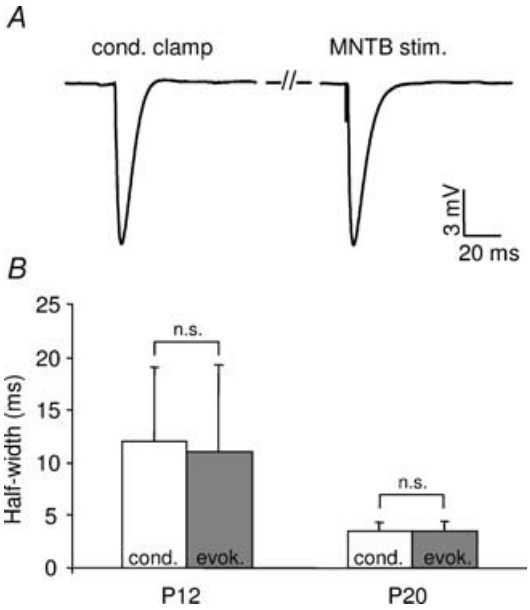

Figure 6. Simulated *versus* evoked IPSPs
A, recordings of IPSPs evoked by injection of a simulated inhibitory conductance (cond. clamp) and during stimulation of the MNTB fibres (MNTB stim.) in the same P12 MSO principal cell. The sample trace represents an average of 25 responses and has been truncated in the middle. *B*, mean half-widths of IPSPs during conductance clamp (cond.) and MNTB fibre stimulation (evok.) in gerbils aged P12 ($n = 4$) and P20 ($n = 4$), respectively. Error bars represent 95% confidence intervals. n.s., not significant.

© The Physiological Society 2005

was -60 ± 7 mV (mean ± s.d., range −46 mV—77 mV; $n = 71$). This V_{rest} is completely in line with those measured in the LSO of neonatal and juvenile rats (Kandler & Friauf, 1995) and, in the MSO of mature guinea-pigs (Smith, 1995).

The $E_{glycine}$, measured using the gramicidin-perforated patch method (Kyrozis & Reichling, 1995) was also mature at hearing onset, as no difference in the $E_{glycine}$ could be detected between P12 and P21 (Fig. 7). The average $E_{glycine}$ was -90 ± 3 mV (mean ± s.d., range −85 mV to −96 mV; $n = 15$). Such a negative $E_{glycine}$ could potentially enhance the effect of glycinergic synaptic inputs to the MSO principal cells. An equally negative $E_{glycine}$ has also been demonstrated for mature cerebellar Purkinje cells (Chavas & Marty, 2003).

Acoustic experience changes the properties of the glycinergic inputs

During a critical period after hearing onset, the glycinergic receptors are reorganized from the dendrites to the soma. This development depends on a normal acoustic experience and is significantly reduced if animals are reared in omnidirectional noise during hearing onset (Kapfer *et al.* 2002). Accordingly, the effect of omnidirectional noise exposure on the amplitudes and kinetics of glycinergic currents after hearing onset was investigated at P17–P20. One of the major findings was a large increase in the IPSC peak conductance. The IPSC peak conductance, evoked by maximal stimulation (~4 times threshold), was more than two-fold larger in noise-reared animals (28.8 ± 15.3 nS; mean ± s.d.; P17–P20, $n = 14$) compared with age-matched controls (11.4 ± 6.9 nS; mean ± s.d. $n = 12$, $P = 0.002$), whereas no difference was observed between noise-reared and P12 animals (23.7 ± 11.4 nS; mean ± s.d., $n = 23$, $P = 0.26$) (Fig. 8*A* and *C*). This effect was paralleled by a significantly higher mIPSC frequency in the noise-reared (96 ± 61 events min^{-1}; mean ± s.d., $n = 6$) and P12 gerbils (87 ± 35 events min^{-1}; mean ± s.d., $n = 11$) when compared to P17–P20 animals (32 ± 20 events min^{-1}; mean ± s.d., $n = 10$; $P = 0.003$ and $P < 0.001$, respectively) (Fig. 8*B* and *D*). The differences in IPSC amplitude and mIPSC frequency between noise-reared, young and older animals may depend on the number of release sites, the synaptic release probability or a combination of both these factors. However, the paired pulse ratio of IPSCs was not significantly different between noise-reared (0.80 ± 0.11, mean ± s.d., $n = 7$), P12 (0.88 ± 0.23, mean ± s.d., $n = 7$; $P = 0.41$) or P17–P20 (0.82 ± 0.15, mean ± s.d., $n = 7$; $P = 0.77$) animals (Table 1), which indicates a higher number of release sites rather than an increased release probability in young and noise-reared animals. In addition, the mean amplitudes of the mIPSCs were 11% of the IPSC peak amplitudes in both noise-reared and young animals, whereas the mIPSC amplitudes were 31% of the IPSCs in older gerbils (Table 1). This reflects a decrease in the mean quantal content after hearing onset, which is prevented by rearing the animals in omnidirectional noise.

The effect of noise-rearing on the IPSC kinetics was less pronounced. The τ_{decay} of the evoked IPSCs in noise-reared animals (2.6 ± 0.6 ms, mean ± s.d., $n = 14$) was slightly

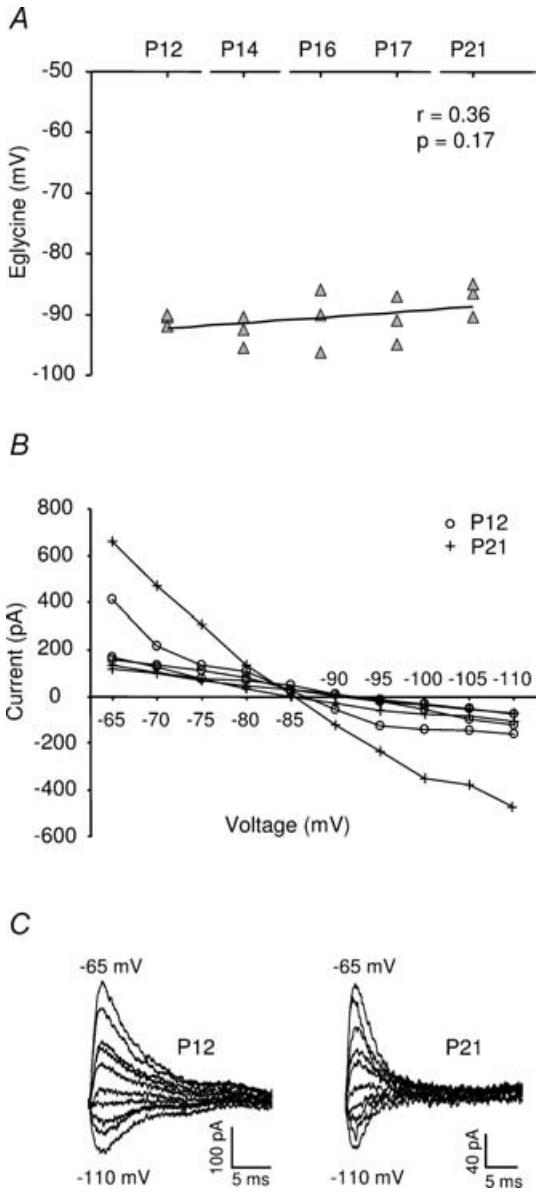

Figure 7. The physiological glycine reversal potential
A, the glycine reversal potential ($E_{glycine}$) *versus* age after hearing onset in gerbils. The continuous line represents a linear regression fit and the *P*-value was obtained with the Pearson test. *B*, the current–voltage relationship of evoked IPSCs during gramicidin perforated patch recordings in P12 ($n = 3$) and P21 ($n = 3$) gerbils. *C*, examples of evoked IPSCs obtained with gramicidin perforated patch recordings at P12 and P21. Holding potentials were set at 5 mV intervals from −65 mV to −110 mV. The stimulus artefact has been deleted.

© The Physiological Society 2005

slower than in age-matched controls (2.2 ± 0.5 ms, mean ± s.d., $n = 29$; $P = 0.01$) (Table 1). However, since there was no difference in the kinetics between the evoked IPSCs and mIPSCs in noise-reared animals ($P = 0.51$ and $P = 0.23$, respectively), this was probably not caused by a higher degree of asynchronous release. Further, there was no change in the kinetics between mIPSCs of noise-reared animals when compared with controls (Table 1).

The time-course of IPSPs in control and noise-reared animals was compared. Since a significant part of the glycinergic inputs remains on the dendrites in noise-reared animals (Kapfer *et al.* 2002), IPSP kinetics could be distorted by dendritic filtering and active conductances located on the dendrites. However, in line with our conductance-clamp experiments, IPSPs of P17 control animals (half-width = 4.6 ± 2.8 ms and 10–90% rise time = 0.78 ± 0.44 ms, $n = 10$) were not faster than those measured in P17 noise-reared animals (half-width = 4.9 ± 2.6 ms and 10–90% rise time = 0.99 ± 0.23 ms, $n = 7$; p = 0.43 and $P = 0.23$, respectively), which presumably have a substantial inhibitory input to the dendrites.

The glycinergic currents are equally fast in the MSO and the LSO

The LSO, an adjacent nucleus mainly involved in the processing of interaural intensity differences, also receives

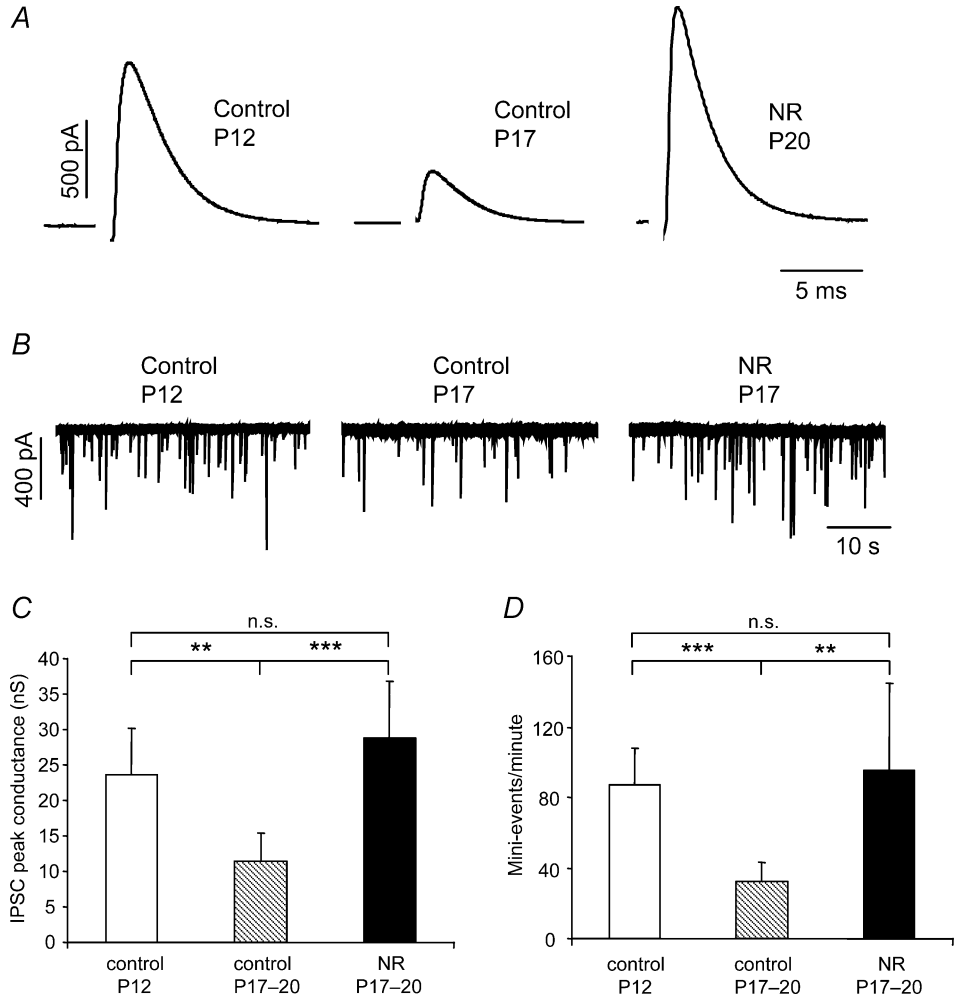

Figure 8. Comparison of glycinergic IPSC properties in control and noise-reared (NR) gerbils
A, examples of evoked IPSCs, evoked by maximal stimulation, in control animals at P12, P17 and in a NR animal (P20). Note the >2-fold increase in peak amplitude in the NR compared to the control animals. Sample records represent an average of >20 responses. The stimulus artefact has been deleted. *B*, sample traces of mIPSCs recorded in the presence of TTX (1 μM) in control animals (P12: 88 events min^{-1} and P17: 28 events min^{-1}) and in a NR gerbil (P17: 75 events min^{-1}). Note the >2.5-fold higher mIPSC frequency in NR compared to control animals *C*, the mean IPSC peak conductance in controls (P12; $n = 13$ and P17–P20; $n = 12$) and in NR animals (P17–P20; $n = 14$). *D*, the mean frequency of mIPSC events in controls (P12; $n = 11$ and P17–P20; $n = 20$) and in NR (P17–P20; $n = 6$) animals. Error bars represent 95% confidence intervals. $^{**}P < 0.01$, $^{***}P < 0.001$.

© The Physiological Society 2005

Table 1. Summary of the time-course of glycinergic synaptic currents in the MSO

	P12	P17–P20	NR P17–P20	P12 *versus* P17–20	P12 *versus* NR P17–P20	P17–20 *versus* NR P17–P20
mIPSC						
τ_{decay} (ms)	2.3 ± 0.25	2.5 ± 0.30	2.4 ± 0.75	n.s.	n.s.	n.s.
Rise time (ms)	0.34 ± 0.06	0.33 ± 0.04	0.36 ± 0.05	n.s.	n.s.	n.s.
Amplitude (nS)	2.3 ± 0.65	3.6 ± 0.58	3.3 ± 1.2	**	n.s.	n.s.
Events min^{-1}	87 ± 21	32 ± 10	96 ± 49	***	n.s.	**
IPSC						
τ_{decay} (ms)	4.0 ± 1.1	2.2 ± 0.18	2.6 ± 0.31	***	*	**
Rise time (ms)	0.70 ± 0.15	0.45 ± 0.07	0.43 ± 0.09	**	*	n.s.
Peak conductance (nS)	23.7 ± 4.7	11.4 ± 3.9	28.8 ± 8.0	**	n.s.	***
Mean paired pulse ratio	0.88 ± 0.17	0.82 ± 0.11	0.80 ± 0.08	n.s.	n.s.	n.s.
Mean quantal content	9.1	3.2	8.7			

Values are mean ± 95% confidence intervals determined for miniature (mIPSCs) and IPSCs in control (P12 and P17–P20) and noise-reared gerbils (P17–P20) at 32°C. The τ_{decay} values are estimated by fitting a single exponential function to averaged responses, and the corresponding rise times are measured as the 10–90% rise time of the same response. Peak conductances represent the averaged response evoked by maximal stimulation of the MNTB fibre bundle. The ratio between the mean mIPSC amplitude and the mean IPSC peak conductance represents the mean quantal content. The mean paired pulse ratio ($IPSC_2 \times IPSC_1{}^{-1}$) was obtained with a stimulus interval of 30 ms. The level of significance between the groups was determined by using Student's unpaired *t* test (*$P < 0.05$, **$P < 0.01$, ***$P < 0.001$; n.s. not significant). The *n*-values for each group are stated in the Results section.

a major glycinergic input from the MNTB (Moore & Caspary, 1983; Spangler *et al.* 1985). In fact, MSO and LSO inputs may be derived from the same subpopulation of MNTB cells (Kuwabara & Zook, 1992). Pharmacological isolation of MNTB fibre-evoked glycinergic IPSCs in LSO principal cells at P17 (Fig. 9*A*) revealed an almost identical response pattern to the IPSCs in the MSO principal cells at the corresponding age with a τ_{decay} of 1.99 ± 0.31 ms ($P = 0.98$) (Fig. 9*B*) and a 10–90% rise time of 0.44 ± 0.10 ms ($P = 0.92$; mean ± s.d., $n = 7$) (Fig. 9*C*).

Finally, a comparison was performed between glycinergic IPSCs in the MSO that had been evoked by two sources of glycinergic inhibition, i.e. by MNTB or LNTB fibre stimulation. Stimulation of LNTB fibres yielded a similar time-course for both IPSPs and IPSCs as those evoked by MNTB fibre stimulation at an age of P17 (Fig. 9*B* and *C*).

Discussion

This study demonstrates striking, experience-dependent adjustments of the glycinergic inhibitory inputs to the MSO after hearing onset. The evoked IPSCs and IPSPs develop fast kinetics, which reach maturity five days after hearing onset. The developmental acceleration of glycinergic inhibition in the MSO is probably related to an increased synchrony of glycine release and a large decrease in input resistance. Moreover, older animals have a much lower mIPSC frequency compared to young or noise-reared animals, which is consistent with an experience-dependent reduction in the number of functional glycinergic synapses (Kapfer *et al.* 2002). On a functional level these changes might represent a developmental adjustment to ITD processing as they parallel the maturation of sound localization behaviour in gerbils (Kelly & Potash, 1986).

Factors governing the development of the IPSC kinetics

During the third postnatal week, the evoked glycinergic IPSCs in the gerbil MSO developed fast kinetics with an average τ_{decay} of 2 ms and a 10–90% rise time of 0.4 ms. These kinetics were roughly two times faster than those measured at hearing onset (P12). In contrast, rise times and decay kinetics of TTX-isolated mIPSCs did not change during the same period, suggesting an increase in the synchrony of action potential-evoked transmitter release. Asynchronous, multivesicular release around hearing onset is also supported by the fact that inflections were present during the rise of some of the evoked IPSCs at P12, but were not observed in older animals. A relationship between the maturation of synaptic currents and a reduction in transmitter release asynchrony has previously been demonstrated for excitatory synapses involved in temporal processing in the auditory brainstem (Chuhma & Ohmori, 1998; Taschenberger & von Gersdorff, 2000; Brenowitz & Trussell, 2001). However, until now, only a few studies have reported a developmental increase of release synchrony at an inhibitory synapse (Awatramani *et al.* 2005; Kirischuk *et al.* 2005). The release synchrony is determined by presynaptic factors, such as the number and composition of Ca^{2+}- and K^+-channels

© The Physiological Society 2005

(Sabatini & Regehr, 1999). For instance, activation of Kv3-channels at the calyx of Held terminal has been shown to shorten the presynaptic action potential waveform, which in turn influences the amount (Ishikawa *et al.* 2003) and the time-course of transmitter release into the synaptic cleft (Dodson & Forsythe, 2004). Moreover, shortening of the Ca^{2+} influx into the presynaptic terminals helps to maintain high temporal fidelity of transmitter release in hippocampal mossy fibre boutons (Geiger & Jonas, 2000).

Apart from asynchronous release, several other factors can govern the decay of the IPSCs, such as spillover of transmitter from contiguous synapses, clearance of glycine from the synaptic cleft and deactivation or desensitization of the glycine receptor. A developmental increase in the rate of transmitter clearance can probably be ruled out as there is no correlation between the decay time-course and the amplitude of the IPSCs (Silver *et al.* 1996). This is in line with a study of glycinergic synaptic currents in brainstem motoneurones (Singer *et al.* 1998), which showed that a blockade of glycine transporters had no effect on IPSC kinetics in juvenile animals. It is also improbable that the developmental decrease of the IPSC decay is related to the glycine receptor deactivation, as the mIPSCs decay with the same speed in young and more mature animals (Legendre, 1998). Furthermore, since the time-course of desensitization works in the order of 0.5–5 s (Legendre, 2001), and the decay of the IPSCs is unaffected by repetitive stimulation (100–500 Hz; data not shown), desensitization of the glycine receptor seems unlikely to affect the decay time-course of the currents measured in this study.

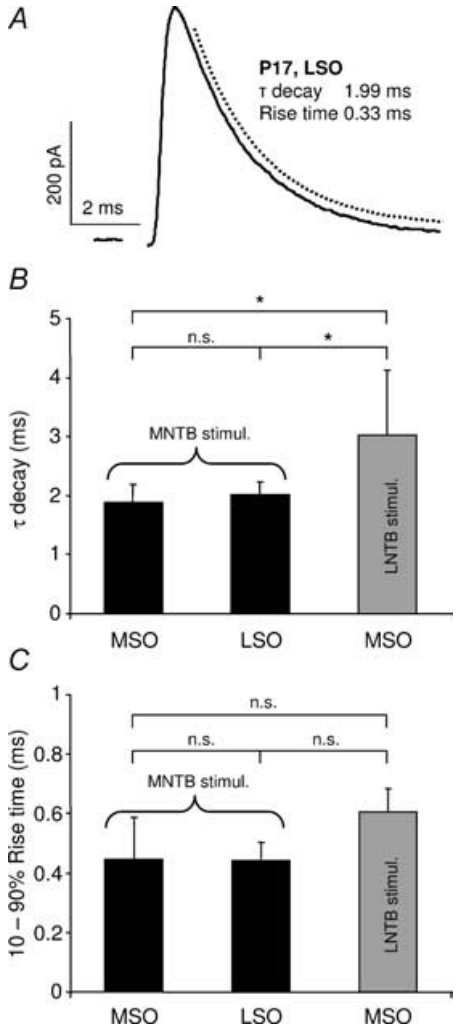

Figure 9. Comparison of glycinergic inputs to the superior olivary complex in P17 gerbils
A, example of an IPSC evoked by MNTB fibre stimulation in an LSO principal cell. The decay time-course was estimated by fitting a single exponential function to the response (broken line). The sample record represents an average of 20 responses. The stimulus artefact has been deleted. *B*, comparison of the mean IPSC τ_{decay} and *C*, the mean 10–90% rise time during MNTB fibre stimulation in the MSO ($n = 8$) and LSO ($n = 7$) or during LNTB fibre stimulation in the MSO ($n = 3$). Error bars represent 95% confidence intervals. n.s., not significant. $^*P < 0.05$.

Implications for the development of the IPSP kinetics

Our results demonstrate not only an acceleration of IPSCs after hearing onset but also a significant shortening of the IPSP half-width and rise time. This effect arises in parallel with a major decrease in input resistance, which indicates that the shortening of synaptic kinetics occurs alongside a shortening of membrane time constants, a process that has also been observed in other parts of the brainstem (Singer *et al.* 1998). Interestingly some neurones developed an extremely low R_{in} ($< 1\,M\Omega$) after hearing onset. We suggest that this is because mature MSO principal cells express voltage-dependent conductances of an unusually large magnitude (unpublished observation), similar to those shown in the octopus cells of the cochlear nucleus (Bal & Oertel, 2000, 2001), and these presumably enhance the encoding of synchronous neuronal activity (Golding *et al.* 1999).

Another factor that has been thought to contribute to the shortening of the IPSPs in the MSO after hearing onset is the refinement of glycine receptors during the same time period, from a mixed somatic-dendritic to a purely somatic location (Kapfer *et al.* 2002). However, the present study indicates that the effect of dendritic filtering is too small to be able to account for the developmental speeding-up of the IPSP time-course. This is in line with the absence of dendritic filtering for the excitatory inputs in the octopus cells of the cochlear nucleus (Gardner *et al.* 1999), which also process acoustic information with extremely high temporal accuracy (Oertel *et al.* 2000). Furthermore, a small effect of dendritic filtering in these neurones is consistent with a recent study, which demonstrated that dendritic filtering only has an effect on IPSP kinetics over much longer dendritic distances (Williams & Stuart,

© The Physiological Society 2005

2003) than the documented extent of MSO principal cell dendrites (Henkel & Brunso-Bechtold, 1990; Kuwabara & Zook, 1999). Why do the inhibitory inputs relocate to the soma in the MSO then? Functionally, it has been shown that somatic inhibition sharpens the time window for coincidence detection of excitatory inputs in several different brain regions such as the auditory brainstem, the hippocampus, the neocortex and the cerebellum (Funabiki *et al.* 1998; Pouille & Scanziani, 2001; Grande *et al.* 2004). In addition, somatic inhibitory synapses would not compete with the excitatory inputs, for which segregation on the dendrites supposedly improves the coincidence detection properties of the cells (AgmonSnir *et al.* 1998). Rearing the animal in omnidirectional noise might disturb the development of segregated inputs by reducing the pruning of inhibitory synapses, and thereby modify the ITD sensitivity in MSO cells (Seidl & Grothe, 2005).

Experience dependent developmental changes of the glycinergic inhibition

This study shows that significant decreases in IPSC peak conductance and mIPSC frequency occur after hearing onset. These developmental changes are prevented if the animals are reared in constant uncorrelated noise, which eliminates the ability to detect ITDs during the critical development of sound localization mechanisms. Since older animals have a much lower mIPSC frequency compared to young or noise-reared animals, and the paired pulse ratio does not differ between these three groups, it favours the hypothesis that the mature MSO principal cells are innervated by only a few glycinergic inputs, whereas young and noise-reared animals, which both have larger peak conductances, have more synapses impinging on these cells. These findings are likely to be related to the activity-dependent pruning of the glycinergic synapses after hearing onset, which has been demonstrated morphologically in the superior olivary complex (Sanes & Takacs, 1993; Koch & Sanes, 1998; Kapfer *et al.* 2002). Fewer synaptic inputs would ensure precise synaptic timing and thereby improve the encoding of auditory cues during the process of ITD coding. There is evidence for developmental reorganization of the MNTB–LSO projections before (Kim & Kandler, 2003; Kandler, 2004) as well as after hearing onset (Sanes & Siverls, 1991). Therefore, the developmental role of acoustic experience might be debatable. However, in line with our data, it has been shown that the development of auditory specificity is highly influenced by temporally (Withington-Wray *et al.* 1990; Nakahara *et al.* 2004) and spectrally (Sanes & Constantine-Paton, 1985; Chang & Merzenich, 2003) structured input activity during a critical period after hearing onset. Moreover, it has recently been shown that the developmental fine tuning of the ITDs of MSO neurones is perturbed by altering the animals' acoustic experience during a critical period after hearing onset (Seidl & Grothe, 2005). These poorly adjusted ITD functions in noise-reared animals may be due to a higher number of MNTB neurones projecting to a single MSO principal cell, resulting in a less synchronized input.

Functional impact of IPSC properties on ITD coding

In several species the most sensitive region of the ITD function, the slope, lies within the physiological range of ITDs, providing maximal resolution of ITD coding (McAlpine *et al.* 2001; Brand *et al.* 2002; Shackleton *et al.* 2003; Hancock & Delgutte, 2004). Seemingly, this is accomplished by glycinergic inhibitory inputs, as iontophoretic administration of strychnine shifts the peak of the ITD function close to the midline and the maximal slope outside the physiological range (Brand *et al.* 2002). As a consequence, the dynamic range of the MSO neurone and thereby also the resolution of ITD coding is highly reduced. In a single compartment model, the shift of the ITD function could be modelled by a very fast inhibitory input ($\tau_{decay} = 0.1$ ms) (Brand *et al.* 2002). However, our results show that the fastest possible time-course of mature glycineric currents peaks around 1 ms in both the MSO and the LSO. These currents are equally fast to those demonstrated in other parts of the brain (Stuart & Redman, 1990), including those obtained from the auditory brainstem of the rat, which is unlikely to use ITDs as a major cue for sound localization (Smith *et al.* 2000; Awatramani *et al.* 2004, 2005). Moreover, the kinetics of the IPSPs in the present study are in line with those measured by intracellular recordings in the MSO *in vitro* (Smith, 1995) and in the LSO *in vivo* (Finlayson & Caspary, 1989) and *in vitro* (Sanes, 1990).

In contrast to the measurements of isolated currents and potentials, studies using multiple inputs implicate that the effective inhibition can be much faster. For instance, *in vivo* characterization of LSO neurones, which receive monaural inhibition from the MNTB and respond to a particular ITD by discharging minimally, have demonstrated that the effect of inhibition can be in the submillisecond range (Joris & Yin, 1995; Park *et al.* 1996; Batra *et al.* 1997). Also, in brain slices of the MSO, it has been shown that the effective time period for suppressing spikes by inhibition is in the same range (Grothe & Sanes, 1994). This discrepancy was recently modelled for the integrated response of excitatory and inhibitory potentials in the LSO (Zhou *et al.* 2005). In line with the studies above, this model predicts that the effective time-window of inhibition can be $\geq$50% shorter than the duration of the underlying inhibitory conductance. The ITD tuning mechanism can also be influenced by input resistance, voltage-dependent rectifying conductances and the geometry of the target neurones (Koch *et al.* 1983; Liu, 2004). These factors may vary between and within

© The Physiological Society 2005

the auditory nuclei (Kandler & Friauf, 1995; Adam *et al.* 2001; Barnes-Davies *et al.* 2004). One explanation for a lateralized ITD function, induced by inhibition, could be an asymmetric distribution of ion channels on the dendrites, which are tuned to the functional voltage range by synaptic inhibition (Svirskis *et al.* 2002). Interestingly, a model incorporating an asymmetric axon origin on the dendrite and sodium channels that are tuned into their functional range by somatic inhibition, requires IPSC kinetics very similar to those of our results to predict the shift of the ITD functions (Zhou *et al.* 2005). However, there are currently no three-dimensional reconstructions of MSO neurones to confirm such an asymmetrical cell structure. To gain further insight into the mechanisms underlying ITD processing, future experiments need to close the gap between measurements of isolated currents and the data obtained during natural sound stimulation, which activates a multitude of inputs interacting in a complex way.

References

Adam TJ, Finlayson PG & Schwarz DW (2001). Membrane properties of principal neurons of the lateral superior olive. *J Neurophysiol* **86**, 922–934.

Adams JC & Mugnaini E (1990). Immunocytochemical evidence for inhibitory and disinhibitory circuits in the superior olive. *Hearres* **49**, 281–298.

AgmonSnir H, Carr CE & Rinzel J (1998). The role of dendrites in auditory coincidence detection. *Nature* **393**, 268–272.

Awatramani GB, Turecek R & Trussell LO (2004). Inhibitory control at a synaptic relay. *J Neurosci* **24**, 2643–2647.

Awatramani GB, Turecek R & Trussell LO (2005). Staggered development of GABAergic and glycinergic transmission in the MNTB. *J Neurophysiol* **93**, 819–828.

Bal R & Oertel D (2000). Hyperpolarization-activated, mixed-cation current (I(h) in octopus cells of the mammalian cochlear nucleus. *J Neurophysiol* **84**, 806–817.

Bal R & Oertel D (2001). Potassium currents in octopus cells of the mammalian cochlear nucleus. *J Neurophysiol* **86**, 2299–2311.

Barnes-Davies M, Barker MC, Osmani F & Forsythe ID (2004). Kv1 currents mediate a gradient of principal neuron excitability across the tonotopic axis in the rat lateral superior olive. *Eur J Neurosci* **19**, 325–333.

Batra R, Kuwada S & Fitzpatrick DC (1997). Sensitivity to interaural temporal disparities of low- and high-frequency neurons in the superior olivary complex. II. Coincidence detection. *J Neurophysiol* **78**, 1237–1247.

Brand A, Behrend O, Marquardt T, McAlpine D & Grothe B (2002). Precise inhibition is essential for microsecond interaural time difference coding. *Nature* **417**, 543–547.

Brenowitz S & Trussell LO (2001). Maturation of synaptic transmission at end-bulb synapses of the cochlear nucleus. *J Neurosci* **21**, 9487–9498.

Cant NB & Benson CG (2003). Parallel auditory pathways: projection patterns of the different neuronal populations in the dorsal and ventral cochlear nuclei. *Brain Res Bull* **60**, 457–474.

Cant NB & Hyson RL (1992). Projections from the lateral nucleus of the trapezoid body to the medial superior olivary nucleus in the gerbil. *Hear Res* **58**, 26–34.

Chang EF & Merzenich MM (2003). Environmental noise retards auditory cortical development. *Science* **300**, 498–502.

Chavas J & Marty A (2003). Coexistence of excitatory and inhibitory GABA synapses in the cerebellar interneuron network. *J Neurosci* **23**, 2019–2031.

Chuhma N & Ohmori H (1998). Postnatal development of phase-locked high-fidelity synaptic transmission in the medial nucleus of the trapezoid body of the rat. *J Neurosci* **18**, 512–520.

Clark GM (1969). The ultrastructure of nerve endings in the medial superior olive of the cat. *Brain Res* **14**, 293–305.

Dodson PD & Forsythe ID (2004). Presynaptic K^+ channels: electrifying regulators of synaptic terminal excitability. *Trends Neurosci* **27**, 210–217.

Finlayson PG & Caspary DM (1989). Synaptic potentials of chinchilla lateral superior olivary neurons. *Hear Res* **38**, 221–228.

Funabiki K, Koyano K & Ohmori H (1998). The role of GABAergic inputs for coincidence detection in the neurones of nucleus laminaris of the chick. *J Physiol* **508**, 851–869.

Gardner SM, Trussell LO & Oertel D (1999). Time course and permeation of synaptic AMPA receptors in cochlear nuclear neurons correlate with input. *J Neurosci* **19**, 8721–8729.

Geiger JRP & Jonas P (2000). Dynamic control of presynaptic Ca^{2+} inflow by fast-inactivating K^+ channels in hippocampal mossy fiber boutons. *Neuron* **28**, 927–939.

Goldberg JM & Brown PB (1969). Response of binaural neurons of dog superior olivary complex to dichotic tonal stimuli: some physiological mechanisms of sound localization. *J Neurophysiol* **32**, 613–636.

Golding NL, Ferragamo MJ & Oertel D (1999). Role of intrinsic conductances underlying responses to transients in octopus cells of the cochlear nucleus. *J Neurosci* **19**, 2897–2905.

Grande LA, Kinney GA, Miracle GL & Spain WJ (2004). Dynamic influences on coincidence detection in neocortical pyramidal neurons. *J Neurosci* **24**, 1839–1851.

Grothe B (2003). New roles for synaptic inhibition in sound localization. *Nat Rev Neurosci* **4**, 540–550.

Grothe B & Sanes DH (1993). Bilateral inhibition by glycinergic afferents in the medial superior olive. *J Neurophysiol* **69**, 1192–1196.

Grothe B & Sanes DH (1994). Synaptic inhibition influences the temporal coding properties of medial superior olivary neurons: an *in vitro* study. *J Neurosci* **14**, 1701–1709.

Hancock KE & Delgutte B (2004). A physiologically based model of interaural time difference discrimination. *J Neurosci* **24**, 7110–7117.

Henkel CK & Brunso-Bechtold JK (1990). Dendritic morphology and development in the ferret medial superior olivary nucleus. *J Comp Neurol* **294**, 377–388.

Ishikawa T, Nakamura Y, Saitoh N, Li WB, Iwasaki S & Takahashi T (2003). Distinct roles of Kv1 and Kv3 potassium channels at the calyx of held presynaptic terminal. *J Neurosci* **23**, 10445–10453.

Joris PX & Yin TC (1995). Envelope coding in the lateral superior olive. I. Sensitivity to interaural time differences. *J Neurophysiol* **73**, 1043–1062.

© The Physiological Society 2005

Kandler K (2004). Activity-dependent organization of inhibitory circuits: lessons from the auditory system. *Curr Opin Neurobiol* **14**, 96–104.

Kandler K & Friauf E (1995). Development of glycinergic and glutamatergic synaptic transmission in the auditory brainstem of perinatal rats. *J Neurosci* **15**, 6890–6904.

Kapfer C, Seidl AH, Schweizer H & Grothe B (2002). Experience-dependent refinement of inhibitory inputs to auditory coincidence-detector neurons. *Nat Neurosci* **5**, 247–253.

Kelly JB & Potash M (1986). Directional responses to sounds in young gerbils (*Meriones unguiculatus*). *J Comp Psychol* **100**, 37–45.

Kim G & Kandler K (2003). Elimination and strengthening of glycinergic/GABAergic connections during tonotopic map formation. *Nat Neurosci* **6**, 282–290.

Kimura T, Sako K, Tanaka K, Kusakabe M, Tanaka T & Nakada T (2002). Effect of mild hypothermia on energy state recovery following transient forebrain ischemia in the gerbil. *Exp Brain Res* **145**, 83–90.

Kirischuk S, Juttner R & Grantyn R (2005). Time-matched pre- and postsynaptic changes of GABAergic synaptic transmission in the developing mouse superior colliculus. *J Physiol* **563**, 795–807.

Koch C, Poggio T & Torre V (1983). Nonlinear interactions in a dendritic tree: localization, timing, and role in information processing. *Proc Natl Acad Sci U S A* **80**, 2799–2802.

Koch U & Sanes DH (1998). Afferent regulation of glycine receptor distribution in the gerbil LSO. *Microsc Res Tech* **41**, 263–269.

Kuwabara N & Zook JM (1992). Projections to the medial superior olive from the medial and lateral nuclei of the trapezoid body in rodents and bats. *J Comp Neurol* **324**, 522–538.

Kuwabara N & Zook JM (1999). Local collateral projections from the medial superior olive to the superior paraolivary nucleus in the gerbil. *Brain Res* **846**, 59–71.

Kyrozis A & Reichling DB (1995). Perforated-patch recording with gramicidin avoids artifactual changes in intracellular chloride concentration. *J Neurosci Meth* **57**, 27–35.

Legendre P (1998). A reluctant gating mode of glycine receptor channels determines the time course of inhibitory miniature synaptic events in zebrafish hindbrain neurons. *J Neurosci* **18**, 2856–2870.

Legendre P (2001). The glycinergic inhibitory synapse. *Cell Mol Life Sci* **58**, 760–793.

Liu G (2004). Local structural balance and functional interaction of excitatory and inhibitory synapses in hippocampal dendrites. *Nat Neurosci* **7**, 373–379.

McAlpine D & Grothe B (2003). Sound localization and delay lines – do mammals fit the model? *Trends Neurosci* **26**, 347–350.

McAlpine D, Jiang D & Palmer AR (2001). A neural code for low-frequency sound localization in mammals. *Nat Neurosci* **4**, 396–401.

Moore MJ & Caspary DM (1983). Strychnine blocks binaural inhibition in lateral superior olivary neurons. *J Neurosci* **3**, 237–242.

Nakahara H, Zhang LI & Merzenich MM (2004). Specialization of primary auditory cortex processing by sound exposure in the 'critical period'. *Proc Natl Acad Sci U S A* **101**, 7170–7174.

Oertel D, Bal R, Gardner SM, Smith PH & Joris PX (2000). Detection of synchrony in the activity of auditory nerve fibers by octopus cells of the mammalian cochlear nucleus. *Proc Natl Acad Sci U S A* **97**, 11773–11779.

Park TJ, Grothe B, Pollak GD, Schuller G & Koch U (1996). Neural delays shape selectivity to interaural intensity differences in the lateral superior olive. *J Neurosci* **16**, 6554–6566.

Pouille F & Scanziani M (2001). Enforcement of temporal fidelity in pyramidal cells by somatic feed- forward inhibition. *Science* **293**, 1159–1163.

Raman IM, Zhang S & Trussell LO (1994). Pathway-specific variants of AMPA receptors and their contribution to neuronal signaling. *J Neurosci* **14**, 4998–5010.

Sabatini BL & Regehr WG (1999). Timing of synaptic transmission. *Annu Rev Physiol* **61**, 521–542.

Sanes DH (1990). An in vitro analysis of sound localization mechanisms in the gerbil lateral superior olive. *J Neurosci* **10**, 3494–3506.

Sanes DH & Constantine-Paton M (1985). The sharpening of frequency tuning curves requires patterned activity during development in the mouse, *Mus musculus*. *J Neurosci* **5**, 1152–1166.

Sanes DH & Siverls V (1991). Development and specificity of inhibitory terminal arborizations in the central nervous system. *J Neurobiol* **22**, 837–854.

Sanes DH & Takacs C (1993). Activity-dependent refinement of inhibitory connections. *Eur J Neurosci* **5**, 570–574.

Seidl AH & Grothe B (2005). Development of sound localization mechanisms in the mongolian gerbil is shaped by early acoustic experience. *J Neurophysiol* **94**, 1028–1036.

Shackleton TM, Skottun BC, Arnott RH & Palmer AR (2003). Interaural time difference discrimination thresholds for single neurons in the inferior colliculus of guinea pigs. *J Neurosci* **23**, 716–724.

Silver RA, Colquhoun D, Cull-Candy SG & Edmonds B (1996). Deactivation and desensitization of non-NMDA receptors in patches and the time course of EPSCs in rat cerebellar granule cells. *J Physiol* **493**, 167–173.

Singer JH, Talley EM, Bayliss DA & Berger AJ (1998). Development of glycinergic synaptic transmission to rat brain stem motoneurons. *J Neurophysiol* **80**, 2608–2620.

Skottun BC (1998). Sound localization and neurons. *Nature* **393**, 531.

Smith PH (1995). Structural and functional differences distinguish principal from nonprincipal cells in the guinea pig MSO slice. *J Neurophysiol* **73**, 1653–1667.

Smith AJ, Owens S & Forsythe ID (2000). Characterisation of inhibitory and excitatory postsynaptic currents of the rat medial superior olive. *J Physiol* **529**, 681–698.

Spangler KM, Warr WB & Henkel CK (1985). The projections of principal cells of the medial nucleus of the trapezoid body in the cat. *J Comp Neurol* **238**, 249–262.

Spitzer MW & Semple MN (1995). Neurons sensitive to interaural phase disparity in gerbil superior olive: diverse monaural and temporal response properties. *J Neurophysiol* **73**, 1668–1690.

Stuart GJ & Redman SJ (1990). Voltage dependence of Ia reciprocal inhibitory currents in cat spinal motoneurones. *J Physiol* **420**, 111–125.

© The Physiological Society 2005

Svirskis G, Kotak V, Sanes DH & Rinzel J (2002). Enhancement of signal-to-noise ratio and phase locking for small inputs by a low-threshold outward current in auditory neurons. *J Neurosci* **22**, 11019–11025.

Taschenberger H & von Gersdorff H (2000). Fine-tuning an auditory synapse for speed and fidelity: developmental changes in presynaptic waveform, EPSC kinetics, and synaptic plasticity. *J Neurosci* **20**, 9162–9173.

von Gersdorff H & Borst JG (2002). Short-term plasticity at the calyx of held. *Nature Rev Neurosci* **3**, 53–64.

Wall MJ, Robert A, Howe JR & Usowicz MM (2002). The speeding of EPSC kinetics during maturation of a central synapse. *Eur J Neurosci* **15**, 785–797.

Williams SR & Stuart GJ (2003). Voltage- and site-dependent control of the somatic impact of dendritic IPSPs. *J Neurosci* **23**, 7358–7367.

Withington-Wray DJ, Binns KE, Dhanjal SS, Brickley SG & Keating MJ (1990). The maturation of the superior collicular map of auditory space in the guinea-pig is disrupted by developmental auditory deprivation. *Eur J Neurosci* **2**, 693–703.

Yin TC & Chan JC (1990). Interaural time sensitivity in medial superior olive of cat. *J Neurophysiol* **64**, 465–488.

Zhou Y, Carney LH & Colburn HS (2005). A model for interaural time difference sensitivity in the medial superior olive: interaction of excitatory and inhibitory synaptic inputs, channel dynamics, and cellular morphology. *J Neurosci* **25**, 3046–3058.

Acknowledgements

This work was supported by the Alexander v. Humboldt Foundation, the Swedish Medical Research Council, the Max-Planck Society and the Hochschul- und Wissenschaftsprogramm. We thank Drs J. Rothman and A. Klug for comments on an earlier version the manuscript and C. Leibold for discussions. Additionally, we thank the three reviewers whose suggestions greatly improved this manuscript.

© The Physiological Society 2005